UTM UNIVERSITI TEKNOLOGI MALAYSIA
INTERNATIONAL JOURNAL OF INNOVATIVE COMPUTING
ISSN 2180-4370
Journal Homepage : https://ijic.utm.my/

Proposed DeepFake Detection Method Using Multiwavelet Transform

Saadi Mohammed Saadi
Informatics Institute for Postgraduate Studies
Iraqi Commission for Computers and Informatics
Baghdad, Iraq
Email: phd202130692@iips.icci.edu.iq

Waleed Ameen Mahmoud Al-Jawher
Department of Electronics and Communication Engineering
Uruk University
Baghdad, Iraq

Submitted: 30/11/2022. Revised edition: 31/3/2023. Accepted: 31/3/2023. Published online: 13/9/2023
DOI: https://doi.org/10.11113/ijic.v13n1-2.420

***Abstract*—Videos made by artificial intelligence (A.I.) seem real, but they are not. When making DeepFake videos, face-swapping methods are frequently employed. The misuse of technology when using fakes, even though it was fun at first, these videos were somewhat recognizable to human eyes. However, as machine learning advanced, it became simpler to produce profound fake videos. It's practically impossible to tell it apart from actual videos now. Using GANs (Generative Adversarial Networks) and other deep learning techniques, DeepFake videos are output technology that may mislead people into thinking something is real when it is not. This study used a MultiWavelet transform to analyze the type of edge and its sharpness to develop a blur inconsistency detecting system. With this capability, it can assess whether or not the facial area is obscured in the video. As a result, it will detect fake videos. This paper reviews DeepFake detection techniques and discusses how they might be combined or altered to get more accurate results. A detection rate of more than 93.5% was obtained, which is quite successful.**

***Keywords*—DeepFake Video, Generative Adversarial Networks (GAN), MultiWavelet, Artificial Neural Network**

I. INTRODUCTION

GAN is a set of affiliate algorithms within machine learning developed in 2014 [1]. Improved image editing methods have made it simpler and more commonplace than ever before to produce fake digital videos. Recent years have decreased the time required to create fake images and videos thanks to the rapid development of cutting-edge technology such as machine learning and computer vision. The process of eliminating the need for editing steps (manual or human) resulted from high-throughput computing. When you use a video of one person as the input target, a new movie with a different person as the source will produce, and the target object changes as the output. DeepFake uses deep neural networks, training them to improvise the head facial expressions of a target face. Videos resulting from counterfeiting operations that can be produced at a high level, convincing, and authentic. To determine if a digital image or video has been a reliable detection approach of A.I. - a doctored image urgently needs to be altered or note [2]. The proposed method used in this paper to demonstrate how well it can distinguish DeepFake movies from real ones. The artificial faces in the original film are subjected to the affine transformation and blur function to match and enhance the source face.

Utilizing the production speed and budget constraints, the strategy is based on the ability of DeepFake videos to generate videos. The DeepFake algorithm can only generate pseudo-faces of the specified size and resolution. Due to the variable region's "region of interest" (ROI) and the surrounding regions' varying resolution and blur, this shift leaves distinct traces. It is possible to identify DeepFake counterfeit videos using this blur inconsistency. We discover the cause of this mismatch by contrasting the ROI of the artificially blurred parts with the surrounding context, specifically reiterating the accuracy and blur inconsistencies in the face transformation. Identifying faces within each frame is the first stage, and features are then retrieved to build transformation matrices that will align the faces with a predetermined composition. The obtained facial image is not blurred. However, some techniques can determine how much blur is present. The MultiWavelet transform is the foundation of the suggested DeepFake detection technique. Using edge sharpness analysis, one can quantify the amount of ROI blurring based on who: edge type, analysis, and how much if artifact effects damage a particular face image by matching a GAN fake face to an avatar. The ability to distinguish between different edge types and capacity to restore sharpness from blurred images are two benefits of the MultiWavelet transform utilized in this method. Additionally, it is rapid and efficient

since it avoids reconstructing the blur matrix function and does not impact the uniform background of faces in the photos.

As shown in Fig. 1, the added build pipeline, the blur irregularity brought by the DeepFake is due to the affine transformations of the prosthetic face. Several studies of implicit resampling detection have been conducted, including [2-4]. Based on the technique, the DeepFake detection approach allowed a direct adjustment by comparing the region of potential composite faces (ROI) with the remainder of the image, in contrast to earlier algorithms, which frequently attempted to estimate the sample of the full image (the background). The experience should not be blurry or slightly blurry (ROI). The MultiWavelet transform is used in this research to present a new DeepFake detection technique. This technique uses the MultiWavelet transform's capacity to distinguish between various edge types and calculates the amount of blur based on edge sharpness analysis, which will serve as a sign of video frame manipulation.

It was noticed that, when using MultiWavelet to detect the edges of the image (Region of interest and the rest), the detection results were deeper and more accurate in displaying details compared to using Haar wavelet transform, and thus positively affected the decision-making in differentiating between real or fake video.

Divide the rest of the paper into sections: Part II of the presentation covers related work, and Fig. 1 depicts the DeepFake algorithm in general. Part III of the method's explanation includes a classification edge of a diagram, as shown in Fig. 2. Part IV of Fig. 3 displays the inconsistent blur for the construction pipeline. Which also reveals the method's algorithmic processes. Fig. 4 shows how MultiWavelet used to identify DeepFakes. Part V contains the experimental results, and Figs. 7 and 8 show an example of the suggested method.

II. Related Works

D.G and E.J [3] proposed the automatically detection of fake videos. You can use it to get the frame-level properties of a Convolutional Neural Network (CNN) system. Then, to detect manipulations, trained a recurrent neural network (RNN) depending on these features. We contrast our method with a vast collection of DeepFake videos from different video sources. We use a straightforward architecture to show how our system can complete this task with competitive results. Whether or not a video clip has been accurately modified can be determined using less than two seconds of video data, according to experimental results presented which using a large set of manipulated videos. Y. Tu, and X [4], Explain how to use a frame-level convolutional neural network to extract data (CNN). After that, I used the GRU convolutional training method to learn to distinguish between fake and real videos using these attributes. The most recent Celeb-DF datasets (v2), which include an advanced degree from the American University in Cairo, are used for assessment. The findings indicate that the chosen strategy performed better, at 89.3%. According to our theory, faces in the deep phantom film's n and (n + 1) frames are inconsistent,.

Bansal *et al.* [5]. To combine spatial and temporal data, consider using conditional generative adversarial networks. Recycle-GAN improved on previous versions. Davide *et al.* [6] indicate a camera noise print extraction method that enhances model-related artifacts while suppressing scene content. Training a Siamese network using pairs of image corrections from the same (label +1) or different cameras (label -1). Although there are many forensic uses for noise prints, in this study, we concentrate on the location of picture forgeries. Using the forensic community's more popular datasets in experiments revealed that noise print-based techniques offered state-of-the-art performance. Zhou *et al.* [7] discussed Face modification detection using two-stream CNN in this study. The process of creating a new data set to test with several post-processing techniques applied to the segmented region. I support using two-stream CNN for Face Manipulation Detection. Because it could learn how to manipulate effects and the characteristics of lingering hidden noise, the experimental findings of this method were superior to those of other ways.

Because the method used in this work needs to extract the features of the cloaking analysis of the triangular network, the comprehensive engineering design is worth investigating. It will be one of the main directions of future research. The authors Y. Li M *et al.* [8] note that DeepFake films lack realistic eye blinking because training photos, used as a source, typically do not contain images of people with closed eyes. In DeepFake footage, the CNN/RNN model detects the absence of eye blinking. However, purposely combining photos during training with faces that have their eyes closed may be readily revoked by the method of detection CNNs. The authors D. Afshar *et al.* [9] suggested approach focuses primarily on Deepfake and Face2Face, two contemporary techniques that have been exploited to produce compelling fake videos. It offers a mechanism for automatic and effective detection of face manipulation in videos. Videos typically do not lend themselves well to traditional image forensic techniques because of the considerable data degradation caused by compression. To concentrate on the intermediate qualities of images, two networks with a few layers are introduced using a deep learning approach. By analyzing these quick networks on the existing data set and the data set, we created from web videos. Over 98% of DeepFakes and 95% of face-to-face fakes are successfully detected in tests.

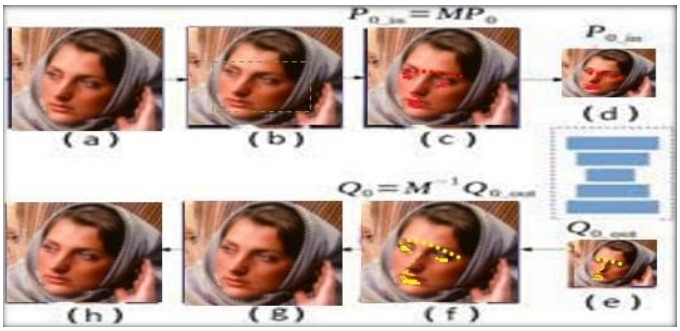

Fig. 1. A description of the DeepFake algorithm. In this case, the source face (a) and (b) The edge of the face has been determined. There have been landmarks identified in (c). (d) After being cut, the appearance is quirky and uniform.. DeepFake face made (e). (f) A face transformation takes place. (g) Real-world landmarks are used to fine-tune the synthetic face (c). The original image combines the fabricated look (g,h)

III. Detection of the Blur Edges to DeepFake Detection

Both direct and indirect methods can estimate the extent of the blur. The following equation describes the linear blur image:

$$a = b * S + N \quad (1)$$

The process represents the noisy image with a, S, and N matrices, and the b matrix represents the blur function. When the b matrix is anonymous, the blur reconstruction function, which includes blur identification and estimation, is reliant on it. Rahtu E. *et al*. proposed a local phase estimation process for studying blur-insensitive images [15th]. Using defocusing spatial contrast estimation from a single image, Kerouh F. *et al*. [17], suggest detecting a tampered and generated image in general. One can directly quantify the blur function extent by experimenting with some identifying aspects of an input image. One of the most versatile features is the edge feature. The edge sharpness and edge type will vary when the blur is present, indicating whether or not to modify the facial image. Dirac, Step, and Roof-Structure are three primary types of edges [18]. According to Fig. 2, the second type is split into "A Step-Structure" and "G Step-Structure." Depending on the intensity shift, it will either be progressive or not [19], [20]. However, every image contains roughly all different kinds of edges, and the majority of the first and third structures are sufficiently sharp. The edges become less crisp if it is smudged. Where (α) is a measurement for the sharpness parameter, which is used to determine whether or not a facial image is blurry using the Dirac structure and A Step-Structure. A blur extent is determined by taking the sharpness of the roof structure and G step structure into account. The parameter α ($0 < \alpha < \pi / 2$) indicates the sharpness of the edge; a bigger value for the sharpness parameter () denotes a sharper edge.

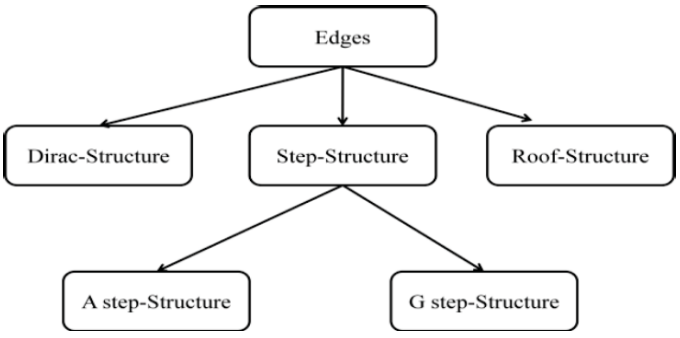

Fig. 2. Classifying edges.

Based on the opacity extent value indicated by the first or second structure, our approach decides whether a given image is blurred or not. As for the percentage of G Step structures, the third structures are likely to be in a blurred vision. By contrasting the amount of blurring (ROI) with the overall amount, we can tell if images (video frames) have been manipulated or not.

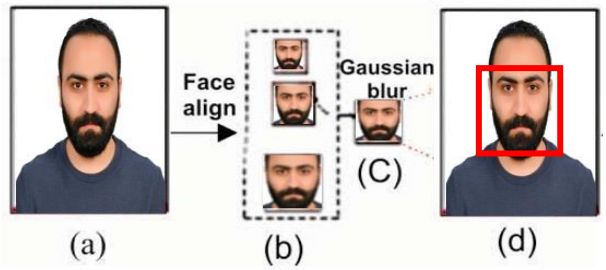

Fig. 3. (a) The original image ;(b) A face aligned at various scales; (c) The choice of an arbitrary scale and the use of Gaussian blur; (d) A distorted affine image with a low value for the sharpness parameter

IV. Proposed DeepFack Detection Algorithm

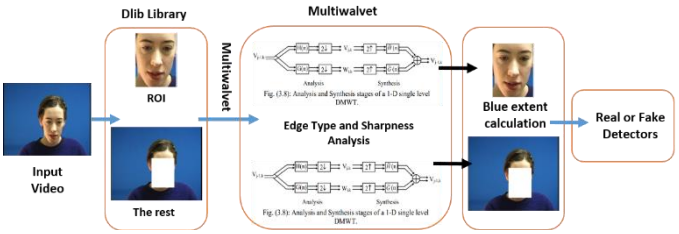

Fig. 4. Proposed DeepFake detecting system's work diagram

DeepFake operation in the above algorithm using MultiWavelet Transformation and Edge Detection, where the proposed method represents the steps shown in Fig. 5 and to implement the proposed method efforts of the following approach to find DeepFake, as shown in Fig. 6.

Proposed DeepFake Detection

1- Face region is recognized and retrieved from the source photos. use the Dlib software suite.
2- Perform Multiwavelet Transform to the (ROI) found in 1st step and the original image.
3- Constructs the edge map (E_{map}) in each scale from detailed sections, as shown below:
$E_{map\,i}(k,l) = \sqrt{LH^2 + HL^2 + HH^2}$ where i = 1,2,3 (2)
4- Divide the edge maps to get the local maxima for each window. The smallest size on the largest window scale is (22), followed by (44), and (88). The result is represented as Emax I (where I = 1, 2, 3).
Emaxi is a measure of edge strength; the higher the value of Emaxi, the stronger the edge's intensity.
5- Specific threshold value is classified as an edge point if Emax I (k, l) > threshold (k, l); otherwise, it is a non-edge point. Let Nedge represent their combined number.
Let N_{edge} be the total number of them.
6- Find all of the image's edge points for each of the edge points (k, l) (the Dirac-Structure and the A Step-Structure). If (k, l) is either a Roof-Structure or a G Step-Structure, then the $E_{max\,1}$ (k, l) > $E_{max\,2}$ (k, l) > $E_{max\,3}$ (k, l) condition holds. Let Nda represent their total number.
7- Find all the roof structure points if (k, l) is a roof structure and $E_{max\,2}$ (k, l) > $E_{max\,1}$ (k, l) and $E_{max\,2}$ > $E_{max\,3}$. Let Nrg represent their combined number.
8- Find all G Step-Roof-Structure- Structure edge points that no longer have a sharp edge. If $E_{max\,i}$ (k, l) threshold, (k, l) is more likely to be in a blurred image for each edge point (k, l). Let N_{br} represent their overall number.
9- Calculate the ratio of all the edges (Dirac and A Step structures), per = $=\frac{N_{da}}{N_{edge}}$; if Per MZero, the image is considered blurry; otherwise, it is not; MZero is a positive integer that is quite close to zero.
10- Use Blur Extent $=\frac{N_{Brg}}{N_{rg}}$ to determine the blurring extent. It shows the confidence coefficient for image blur.
11- Compare the Blur Extent of (ROI) with the remainder of the image if the blur is discovered in (ROI).
12- Finding the source image Determine whether the input frame is authentic or false based on step 11

Fig. 5. The implementation of the steps for the proposed method

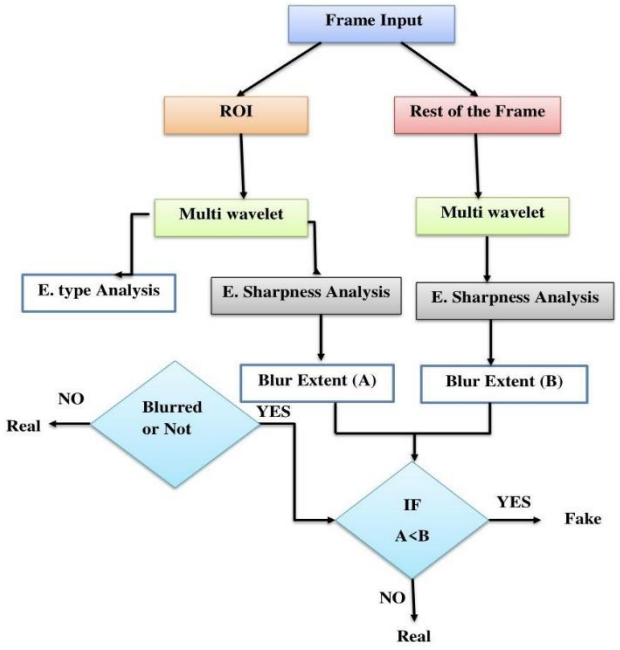

Fig. 6. Proposed DeepFake detection algorithm using MultiWavelet

A. How Does Blur Affect Different Edges?

Because digital camera photos frequently have low noise ratios, the noise component N in "(1)" can be ignored. Utilizing convolution in the initial blur function H impacts the equation and alters the edge property. Remember that the blurred image will not contain a Dirac or A Step structure. On the other hand, Roof and G-step frames will frequently become less sharp (less value).

B. Detection of sharpness and edge type

The popularization of scalar waves gave rise to the concept of MultiWavelet. There are several uses of scaling and wavelet functions rather than just one. Wavelet construction hence has more flexibility. Multiple waves are essential for signal processing because they allow the simultaneous use of compressed support, orthogonality, symmetry, vanishing moments, and short support in contrast to scalar waves. The MultiWavelet Transform provides the best multi-precision analysis capability. F. Tallavó *et al*. [23], to determine both the edge of the Dirac structure and the step structure, used modulus-discrete wave (MASW), which indicates the ability to detect the region of irregular forms through the local maximum wavelet transformation. In the end, MASW is a waste of time. The basis of the proposed method is multi-wave transduction (MWT). Functions derived from sampling the Multiwavelet functions at 2n places are known as MultiWavelet functions. The function can conveniently represent in a matrix form. The basis for finding the sequence M.W. (w, t) in each row of the matrix H (n), where the index (w) is the number of M.W. ژfunctions and index (w) is the discrete point of the function determination interval (t). Employing the recurrence relation presented below can construct any dimension of the MultiWavelet matrix. [24-31].

One kind of transformation that may apply to compress images is the wavelet transform. Wavelets and MultiWavelets are pretty similar, yet they also differ significantly. The process of wavelet interpretation using polycyclic analysis with the wavelet function. Indeed, multimeter (and wavelet) functions are possible - the central tenet of MultiWavelets. From the set of wavelet functions, the process of defining a MultiWavelets function as MultiWavelets. When r = 1, it is referred to as a scalar wavelet or simply a wavelet. Although r can theoretically be any value, most MultiWavelets studied thus far have r = 2. [25-27]. Scalar wavelet transforms matrices as shown in Fig. 7 for computing discrete MultiWavelets transform:

$$W = \begin{bmatrix} H_0 & H_1 & H_2 & H_3 & 0 & 0 & \cdots & 0 & 0 & 0 & 0 \\ 0 & 0 & H_0 & H_1 & H_2 & H_3 & \cdots & 0 & 0 & 0 & 0 \\ \vdots & \vdots & \vdots & \vdots & \vdots & \vdots & \cdots & \vdots & \vdots & \vdots & \vdots \\ H_2 & H_3 & 0 & 0 & 0 & 0 & \cdots & 0 & 0 & H_0 & H_1 \\ G_0 & G_1 & G_2 & G_3 & \vdots & \vdots & \cdots & 0 & 0 & 0 & 0 \\ 0 & 0 & G_0 & G_1 & G_2 & G_3 & \cdots & 0 & 0 & 0 & 0 \\ \vdots & \vdots & \vdots & \vdots & \vdots & \vdots & \cdots & \vdots & \vdots & \vdots & \vdots \\ 0 & 0 & 0 & 0 & 0 & 0 & \cdots & G_0 & G_1 & G_2 & G_3 \\ G_2 & G_3 & 0 & 0 & 0 & 0 & \cdots & 0 & 0 & G_0 & G_1 \end{bmatrix}$$

Fig. 7. MultiWavelets transform matrices

To illustrate the impulse responses of low-pass and high-pass filters, respectively, Hi and Gi are processes of low-pass and high-pass filters. Scalar energies differ from multiple sub-bands because multi-wave decomposition consists of two low-passes and two high-pass sub-bands in each dimension. During one stage of decomposition employing a scalar wavelet transform, the 2D picture data is replaced by four blocks corresponding to subbands representing either low-pass or high-pass at both sizes. Utilizing convolution in the initial blur function H impacts the equation and alters the edge property.

V. Results

Testing the proposed method using the DeepFake "UADFV" video dataset. [10]. UADFV's set includes 100 videos, 49 of which and 51 are. Each video clip (12 seconds approx) is approximately (full frames about 35,280). The test results showed that this model could successfully recognize DeepFake video generated by GANs and has a high degree of generalization. In other words, it can quickly and reliably identify pictures and videos produced by different GAN models. The Table I displays the results of the area under the curve (AUC) for the suggested approach and a few additional methods. A test sample demonstrates the proposed method's effectiveness for identifying manufactured pseudo-objects, as shown in Fig. 8. The video has a running time of 292 frames and is one of the "UADFV" datasets (approximately 10 seconds). The findings demonstrate how the blur extent value and ROI bounds diverge (the higher the value, the sharper the edges).

TABLE I. DEEPFAKE METHODS PERFORMANCE COMPARISON

Methods	***"UADFV" dataset***
Two-stream NN [12]	85.1
Meso-4 [17]	84.3
MesoInception-4	82.1
Head Pose [14]	89.0
Proposed Model	91.5

Frames (2) in Fig. 8 can distinguish between the GAN-edited fake image and the difference in blur extent. The blur range values for the two sections are ~22.7 in the left image and differ significantly in the right frame between the ROI and the rest of the picture.

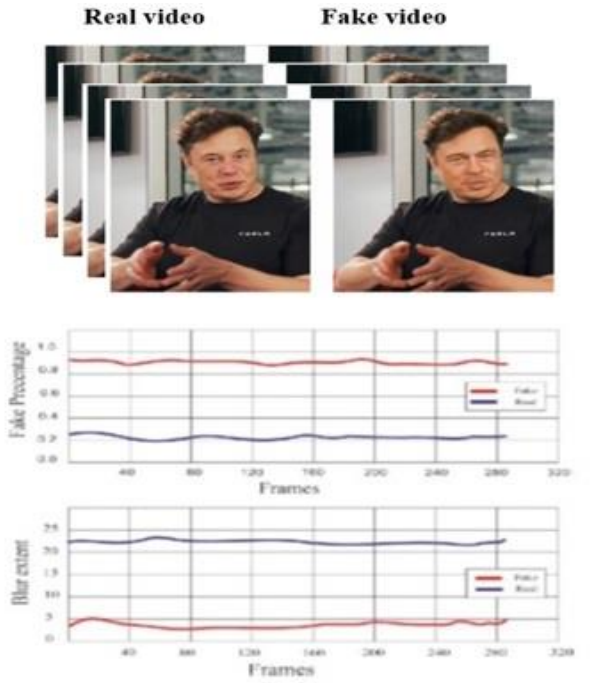

Fig. 8. An example of the suggested method used on a movie made by DeepFake for the "UADFV" dataset

Fig. 9. Recognizing real faces from phony faces

VI. CONCLUSIONS

Any comprehensive strategy or method has yet to offer a genuinely global answer. It is necessary to employ exceptionally impervious methods for everyday picture processing operations, including blurring, scaling, cropping, and rotation. Although correct, some solutions need a lot of resources and computing complexity. Our paper provides a new technique for recognizing DeepFakes; the results were intentionally false face photos or movies. Since the DeepFake method can only generate images of the face with specific dimensions, these images must be modified and blurred to match the appearance in the original movie. Due to the blurred transitions and ROI, different results from DeepFake videos can be effectively recorded using MultiWavelet modulation to identify differences between the ROI and the rest of the image. We tested the effectiveness of our strategy using a set of DeepFake films that have been made publicly available.

ACKNOWLEDGMENTS

The authors would like to thank the Iraqi Commission for Computer and Informatics, as well as the Informatics Institute for Post Grad, for their help and encouragement in performing this work.

REFERENCES

[1] Goodfellow, I., Pouget-Abadie, J., Mirza, M., Xu, B., Warde-Farley, D., Ozair, S., & Bengio, Y. (2020). Generative adversarial networks. *Communications of the ACM*, *63*(11), 139-144.

[2] Dalgaard, N., Mosquera, C., & Pérez-González, F. (2010, September). On the role of differentiation for resampling detection. *2010 IEEE International Conference on Image Processing* (pp. 1753-1756). IEEE.

[3] Kirchner, M. (2008, September). Fast and reliable resampling detection by spectral analysis of fixed linear predictor residue. *Proceedings of the 10th ACM workshop on Multimedia and security* (pp. 11-20).

[4] Kirchner, M., & Bohme, R. (2008). Hiding traces of resampling in digital images. *IEEE Transactions on Information Forensics and Security*, *3*(4), 582-592.

[5] Salim, A. A., Ghoshal, S. K., & Bakhtiar, H. (2021). Tailored morphology, absorption and bactericidal traits of cinnamon nanocrystallites made via PLAL method: Role of altering laser fluence and solvent. *Optik*, *226*, 165879.

[6] Bansal, A., Ma, S., Ramanan, D., & Sheikh, Y. (2018). Recycle-gan: Unsupervised video retargeting. *Proceedings of the European conference on computer vision (ECCV)* (pp. 119-135).

[7] Cozzolino, D., & Verdoliva, L. (2019). Noiseprint: A CNN-based camera model fingerprint. *IEEE Transactions on Information Forensics and Security*, *15*, 144-159.

[8] Zhou, P., Han, X., Morariu, V. I., & Davis, L. S. (2017, July). Two-stream neural networks for tampered face detection. *In 2017 IEEE Conference on Computer Vision and Pattern Recognition Workshops (CVPRW)* (pp. 1831-1839). IEEE.

[9] Li, Y., Chang, M. C., & Lyu, S. (2018, December). In ictu oculi: Exposing ai created fake videos by detecting eye blinking. *2018 IEEE International Workshop on Information Forensics and Security (WIFS)* (pp. 1-7). IEEE.

[10] Salim, A. A., Mahraz, Z. A. S., Anigrahawati, P., Jan, N. A. M., Ghoshal, S. K., Sahar, M. R., ... & Sazali, E. S. (2021). Structural, chemical and magnetic features of gold nanoshapes integrated-Er2O3-doped tellurite glass system prepared by a conventional melt-quenching technique. *Applied Physics A*, *127*(9), 673.

[11] Li, H., Li, B., Tan, S., & Huang, J. (2020). Identification of deep network generated images using disparities in color components. *Signal Processing*, *174*, 107616.

[12] Waheed, S. R., Rahim, M. S. M., Suaib, N. M., & Salim, A. A. (2023). CNN deep learning-based image to vector depiction. *Multimedia Tools and Applications*, 1-20.

[13] Afchar, D., Nozick, V., Yamagishi, J., & Echizen, I. (2018, December). Mesonet: a compact facial video forgery detection network. *2018 IEEE International Workshop on Information Forensics and Security (WIFS)* (pp. 1-7). IEEE.

[14] Güera, D., & Delp, E. J. (2018, November). Deepfake video detection using recurrent neural networks. *2018 15th IEEE International Conference on Advanced Video and Signal based Surveillance (AVSS)* (pp. 1-6). IEEE.

[15] Salim, A. A., Ghoshal, S. K., Suan, L. P., Bidin, N., Hamzah, K., Duralim, M., & Bakhtiar, H. (2018). Liquid media regulated growth of cinnamon nanoparticles: Absorption and emission traits. *Malaysian Journal of Fundamental and Applied Sciences, 14*(3-1), 447-449.

[16] Zhu, X., Cohen, S., Schiller, S., & Milanfar, P. (2013). Estimating spatially varying defocus blur from a single image. *IEEE Transactions on image processing*, *22*(12), 4879-4891.

[17] Kerouh, F., & Serir, A. (2012). A no reference quality metric for measuring image blur in wavelet domain. *International Journal of Digital Information and Wireless Communication*, *1*(4), 767-776.

[18] Salim, A. A., Bakhtiar, H., Krishnan, G., & Ghoshal, S. K. (2021). Nanosecond pulse laser-induced fabrication of gold and silver-integrated cinnamon shell structure: Tunable fluorescence dynamics and morphology. *Optics & Laser Technology*, *138*, 106834.

[19] Lee, J. H., & Ho, Y. S. (2011). High-quality non-blind image deconvolution with adaptive regularization. *Journal of visual communication and image representation*, *22*(7), 653-663.

[20] Abbas, S. I., Hathot, S. F., Abbas, A. S., & Salim, A. A. (2021). Influence of Cu doping on structure, morphology and optical characteristics of SnO_2 thin films prepared by chemical bath deposition technique. *Optical Materials*, *117*, 111212.

[21] Liu, R., & Jia, J. (2008, October). Reducing boundary artifacts in image deconvolution. *2008 15th IEEE International Conference on Image Processing* (pp. 505-508). IEEE.

[22] King, D. E. (2009). Dlib-ml: A machine learning toolkit. *The Journal of Machine Learning Research*, *10*, 1755-1758.

[23] Salim, A. A., Bakhtiar, H., Bidin, N., & Ghoshal, S. K. (2018). Unique attributes of spherical cinnamon nanoparticles produced via PLAL technique: Synergy between methanol media and ablating laser wavelength. *Optical Materials*, *85*, 100-105.

[24] Tallavó, F., Cascante, G., & Pandey, M. (2009). Experimental and numerical analysis of MASW tests for detection of buried timber trestles. *Soil Dynamics and Earthquake Engineering*, *29*(1), 91-102.

[25] Porwik, P., & Lisowska, A. (2004). The Haar-wavelet transform in digital image processing: its status and achievements. *Machine graphics and vision*, *13*(1/2), 79-98.

[26] Waheed, S. R., Suaib, N. M., Rahim, M. S. M., Adnan, M. M., & Salim, A. A. (2021, April). Deep Learning Algorithms-based Object Detection and Localization Revisited. *Journal of Physics: Conference Series* (Vol. 1892, No. 1, p. 012001). IOP Publishing.

[27] Salim, A. A., Ghoshal, S. K., & Bakhtiar, H. (2022). Prominent absorption and luminescence characteristics of novel silver-cinnamon core-shell nanoparticles prepared in ethanol using PLAL method. *Radiation Physics and Chemistry*, *190*, 109794.

[28] Aljewaw, O. B., Karim, M. K. A., Kamari, H. M., Zaid, M. H. M., Salim, A. A., & Mhareb, M. H. A. (2022). Physical and spectroscopic characteristics of lithium-aluminium-borate glass: Effects of varying Nd_2O_3 doping contents. *Journal of Non-Crystalline Solids*, *575*, 121214.

[29] Waheed, S. R., Sakran, A. A., Rahim, M. S. M., Suaib, N. M., Najjar, F. H., Kadhim, K. A., Salim, A. A. & Adnan, M. M. (2023). Design a Crime Detection System based Fog Computing and IoT. *Malaysian Journal of Fundamental and Applied Sciences, 19*(3), 345-354.

[30] Kadhim, K. A., Najjar, F. H., Waad, A. A., Al-Kharsan, I. H., Khudhair, Z. N., & Salim, A. A. (2023). Leukemia Classification using a Convolutional Neural Network of AML Images. *Malaysian Journal of Fundamental and Applied Sciences, 19*(3), 306-312.

[31] Waheed, S. R., Saadi, S. M., Rahim, M. S. M., Suaib, N. M., Najjar, F. H., Adnan, M. M., & Salim, A. A. (2023). Melanoma Skin Cancer Classification based on CNN Deep Learning Algorithms. *Malaysian Journal of Fundamental and Applied Sciences, 19(*3), 299-305.